

Chapter

The Ionizing Radiation Interaction with Matter, the X-ray Computed Tomography Imaging, the Nuclear Medicine SPECT, PET and PET-CT Tomography Imaging

Evangelos Gazis

Abstract

The mechanism of the ionizing radiation interaction with matter is described for heavy charged particles, electrons and photons. Those effects causing energy loss of the radiation with sequential effects of absorption or attenuation are presented. The features of some characteristic detector systems with the relative electronics and the data acquisition system (DAQ) are presented. Those detectors are related with the medical imaging sensor systems. The characteristics of the medical imaging process of the X-ray and nuclear imaging with SPECT, PET and the combination of PET-CT are presented. The computed X-ray tomography, called CT, and the nuclear medicine tomography are presented, implementing the most of the previous parts, as they are defined in PET and SPECT imaging plus the combination of PET with CT the PET-CT.

Keywords: ionizing radiation, X-ray imaging, nuclear medicine, PET, SPECT, PET-CT imaging

1. Introduction

The approach of this chapter is to cover physical principles of the interaction mechanisms of the ionizing radiation, the instrumental detector design and the relative electronics with the data acquisition setup, the image reconstruction techniques, and clinical applications of the imaging techniques most commonly used in clinical medicine as well as in academic research. It starts with the ionizing radiation interaction with matter for various particles and the properties then, the X-ray computed tomography, finishing with the nuclear medicine imaging with SPECT, PET and PET-CT imaging.

2. The ionizing radiation interaction with matter

Unstable nuclei can emit a variety of electrically charged and neutral, particles as well as electromagnetic radiation known as γ -rays (energetic photons).

The best-known particle emission modes are the α -decay, in which a Helium nucleus is produced, and β -decay where an energetic electron e^- (or a positron, e^+) and an anti-neutrino (or a neutrino) are created. All these emissions are generically referred to as nuclear radiation. Their interaction with matter may occur via the electromagnetic, the strong or the weak nuclear forces. An important issue in studying the passage of energetic nuclear radiation through matter is in understanding the transfer of energy produced. Energy transfer mechanisms depend on a number of factors, such as the type of radiation and its energy, as well as the physical properties of the irradiated material. Electrically charged particles, and γ -rays, of nuclear origin interact with highest probability with atomic excitation and ionization. In many of those processes, secondary electrons are produced which spread the energy deposition away from the primary interaction region. Measuring the effects of radiation on matter and finding out the relationship between them and the energy lost by the original radiation is the basis of all nuclear detection methods. When dealing with living matter, the biological impacts of such phenomena are the subject of much concern and study [1–4].

2.1 Interaction of alpha particles

The alpha particles (nuclei of Helium) have two protons and two neutrons bound together. Their mass is relatively large and carries a double positive charge. Alpha particles are commonly spontaneously emitted by the heavy radioactive nuclei occurring in the nature (Uranium, Thorium or Radium), as well as the transuranic elements (Neptunium, Plutonium or Americium). The high mass and charge of an alpha particle, relative to other forms of nuclear radiation, causes its greater ionization power and poorer ability to penetrate matter. A piece of paper can stop them. They travel only a few centimeters but deposit all their energies along their short paths.

2.1.1 Stopping power

The alpha charged particles passing through matter lose kinetic energy by excitation of bound electrons and by ionization. The maximum transferable kinetic energy to an electron depends on the mass m_0 and the momentum of the incident alpha particle. Given the momentum of the incident particle, $p = \gamma m_0 \beta c$, where γ is the Lorentz factor ($= E/m_0 c^2$), $\beta c = v$ the velocity, and m_0 the rest mass; then the maximum transferable energy to electron with mass m_e is

$$E_{kin}^{max} = \frac{2m_e c^2 \beta^2 \gamma^2}{1 + 2\gamma m_e/m_0 + (m_e/m_0)^2} = \frac{2m_e p^2}{m_0^2 + m_e^2 + 2m_e E/c^2} \quad (1)$$

For low energies:

$$2\gamma m_e/m_0 \ll 1 \quad (2)$$

and under the assumption that the incident alpha particles are heavier than electrons ($m_0 > m_e$) Eq. (1) can be approximated by

$$E_{kin}^{max} \approx 2m_e c^2 \beta^2 \gamma^2 \quad (3)$$

The Energy loss for heavy charged particle per unit length $[dE/dx]$, called stopping power, is given by

$$\frac{dE}{dx} \propto \frac{Z^2}{\beta^2} \ln(a\beta^2\gamma^2) \quad (4)$$

Z = atomic number of the material, a = material-dependent constant.

The trajectory of the charged alpha particle is unchanged after scattering, as in the **Figure 1**.

2.1.2 Bethe-Bloch relation

Therefore, the mean energy loss for ‘heavy’ charged particles through the matter is given by the Bethe and Bloch formula [5–8].

$$-\left\langle \frac{dE}{dx} \right\rangle = 2\pi N_A r_e^2 m_e c^2 \rho \frac{Z}{A} \frac{z^2}{\beta^2} \left[\ln \left(\frac{2m_e c^2 \beta^2 \gamma^2}{I^2} \right) - 2\beta^2 - \delta(\beta\gamma) \right] \quad (5)$$

Fundamental constants: r_e = classical radius of electron, N_A = Avogadro’s number.

Absorber medium: I = mean ionization potential, approximately $I = 16Z^{0.9}$ if $Z > 1$, Z = atomic number of absorber, A = atomic weight of absorber, ρ = density of absorber, δ = density correction, z = atomic number of the incident particle.

2.1.3 Range of alpha particles

A heavy charged particle, such as an alpha particle, has a fairly definite range in a gas, liquid, or solid. The particle loses energy, primarily by the excitation and ionization of atoms in its path, occurs in a large number of small increments. The alpha particle has such a large momentum that its direction is not changed appreciably during the slowing processes. Eventually it loses all its kinetic energy and comes to rest. The distance traversed is called the range, and depends on the energy of the alpha particle, the atom density in the material traversed, and the atomic number and average ionization potential of the atoms comprising this material. Integrate over energy loss from the total energy T to the zero, it is obtained the alpha particles range:

$$R(T) = \int_0^T \left[-\frac{dE}{dx} \right]^{-1} dE \quad (6)$$

A plot of the specific ionization (number of ions formed per unit distance of beam path) versus distance from the alpha particle source for a beam of alpha particles is called a Bragg curve, should have the shape shown in **Figure 2**.

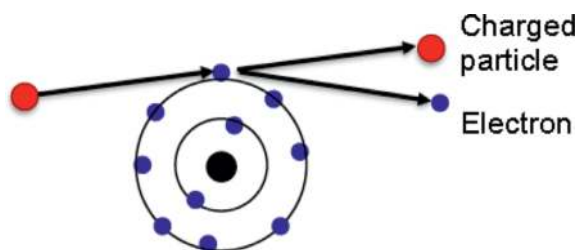


Figure 1.

The alpha particle trajectory remains unchanged after ionizing the atom passing through.

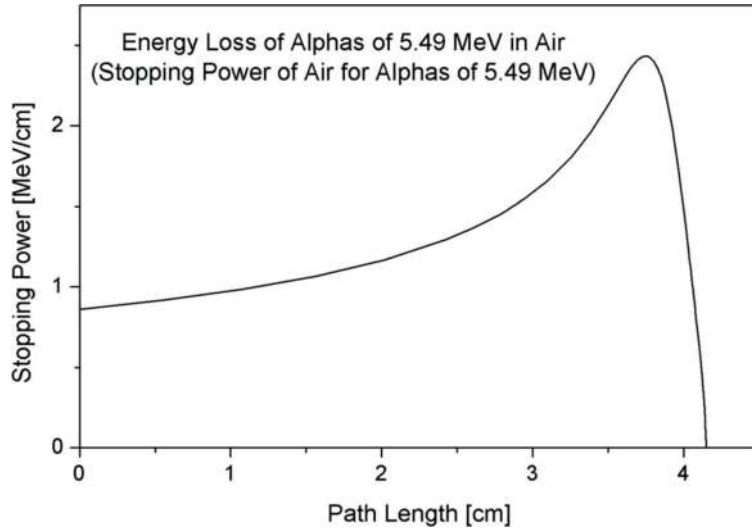


Figure 2.

The alpha particles range in air. The trajectory called Bragg curve has the characteristic peak as the majority of the particles energy is deposited at the last stage of the curve.

2.2 Interaction of electrons and positrons

The interaction of electrons with the matter follows the same mechanism of the charged particles with the absorbed material; taking into account that the incident and target electron have same mass m_e , so the incident and scattering electrons are identical and undistinguishable particles. Electrons as incident particles, however, play a special role in the treatment of the energy loss as the total energy loss of electrons even at low energies (MeV range) is influenced by bremsstrahlung processes. In addition, the ionization loss requires different treatment because the energy-transfer probability must be interpreted in a different way. One electron after the collision receives the energy E_{kin} and the other electron the rest of the energy $E - m_e c^2 - E_{kin}$, where E is the total energy of the incident electron.

The positrons have similar ionization loss as those of the electrons, having these particles are of equal mass, but not identical charge. Under the assumption that the positrons are antiparticles of electrons, there is, however, an additional consideration: if positrons come to rest, they will annihilate with an electron normally into two photons, which are emitted in opposite directions. Both photons have energies of 511 keV in the center-of-mass system, corresponding to the rest mass of the annihilated positron and electron.

2.2.1 Energy loss of electrons/positrons

The energy loss of electrons in the matter can be calculated with the Bethe-Bloch formula, which needs modification, is described by¹

$$-\left\langle \frac{dE}{dx} \right\rangle_{ionization} \propto \ln(E) \quad (7)$$

¹ The exact ionization energy loss of electrons for $z = 1$, is given by $-\frac{dE}{dx} = 4\pi N_A r_e^2 m_e c^2 \frac{Z}{A} \frac{1}{\beta^2} \left[\ln \left(\frac{\gamma m_e c^2}{2I} \right) - \beta^2 - \frac{\delta}{2} \right]$

the parameter δ^* takes different values of the δ for the heavy charged particles.

Dominating process for $E_e > 10\text{--}30\text{ MeV}$ is not anymore ionization but the effect of Bremsstrahlung, where an electron accelerated in the Coulomb field of nucleus produces photon emission

$$-\left\langle \frac{dE}{dx} \right\rangle_{\text{Brem}} \propto \frac{E}{m^2} \quad (8)$$

usually the energy loss due to Bremsstrahlung is written:

$$-\left\langle \frac{dE}{dx} \right\rangle_{\text{Brem}} \propto \frac{E}{X_0}, \quad X_0 = \frac{A}{4aN_A Z^2 r_e^2 \ln \frac{183}{Z^{1/3}}} \quad (9)$$

X_0 = radiation length in $[\text{g}/\text{cm}^2]$.

The physical property of the radiation length for a material is that after passage of one X_0 , the electron has lost all but $(1/e)^{\text{th}}$ of its initial energy [9]

It is also defined a critical energy E_c , for which the energy loss due to ionization is equivalent to energy loss due to Bremsstrahlung:

$$\left. \frac{dE}{dx}(E_c) \right|_{\text{Brems}} = \left. \frac{dE}{dx}(E_c) \right|_{\text{Ion}} \quad (10)$$

In **Figure 3**, the electron energy loss is presented in Copper. The critical energy in this case is about 25 MeV.

2.2.2 Range of electrons/positrons

The range of low-energy electrons ($0.5\text{ MeV} \leq E_{\text{kin}} \leq 5\text{ MeV}$) in Aluminum is described [10] by

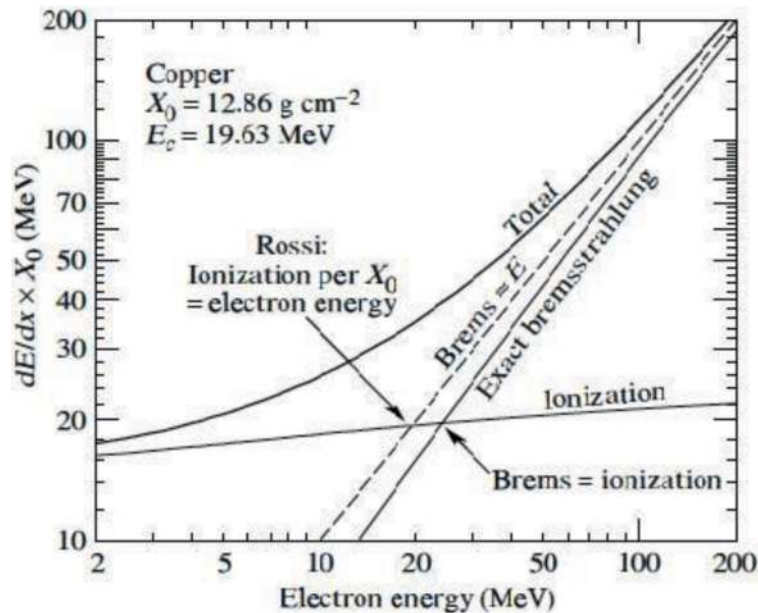


Figure 3.
The electron energy loss is shown under the ionization and the Bremsstrahlung effect for an energy range 2–200 MeV.

$$R_e = 0.526(E_{kin}/MeV - 0.094)g/cm^2 \quad (11)$$

In **Figure 5** the electron range is plotted for various energies of electrons penetrating through a certain Aluminum absorber thickness [10, 11]. This figure shows the difficulty in the definition of a range of a particle due to the pronounced range straggling, in this case mainly due to the fact that electrons will experience multiple scattering and bremsstrahlung in the absorber. The extrapolation of the linear part of the curves shown in **Figure 4** to the intersection with the abscissa defines the practical range [11].

2.3 Linear energy transfer

The term “linear energy transfer (LET)” is used to indicate the average amount of energy that is lost per unit path-length as a charged particle travels through a given material and deposited in it. The LET for electrons is traditionally expressed in units of MeV/cm. In case, the value is divided by the mass density, then in units of MeV-cm²/g. The average amount of energy deposited in a thin sample, per electron, can be estimated by multiplying the LET by the sample thickness. Similarly, the total energy deposited per gram of a specimen, following an exposure of N electrons/area, is

$$E = \frac{LET \cdot N}{\rho} \quad (12)$$

where, ρ is the mass density of the specimen material.

The energy deposited per gram is referred to as the radiation dose. Radiation doses are usually expressed in rads in the older literature, where 1 rad is equal to 100 erg/g. Alternatively the dose is expressed in the Standard International (SI) units of gray (Gy), where 1Gy = 1 J/kg, and thus 1 rad = 0.01 Gy. Since the dose is proportional to the electron exposure, it is commonly used to refer to the exposure as being the “dose.” While this terminology is not strictly correct, the intended meaning becomes understandable in context.

2.4 Interaction of photons: attenuation

Photons are detected indirectly via interactions in the material passed through. Subsequent ionization in the matter provides charged particles, which are spread

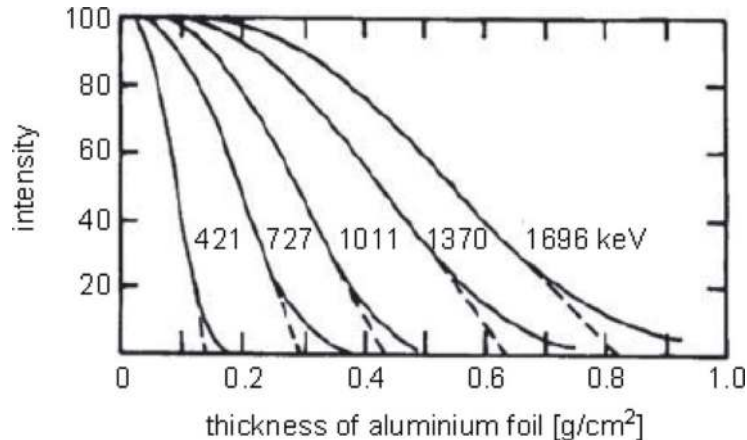


Figure 4.
Absorption of electrons of various energies in aluminum foils [10, 11].

through. Interactions of photons are fundamentally different from ionization processes of charged particles because in every photon interaction, the photon is either completely absorbed (photoelectric effect, pair production) or scattered through a relatively large angle meaning the Compton effect. Since the absorption or scattering is a statistical process, it is impossible to define a range for γ rays. A photon beam is attenuated exponentially in matter according to.

$$I = I_0 e^{-\mu x} \quad (13)$$

The length x in Eq. (13) is an area density with the unit g/cm^2 . If the length is measured in cm, the mass attenuation coefficient μ must be divided by the density ρ of the material. The mass attenuation coefficient μ is related to the cross sections for the various interaction processes of photons according to

$$\mu = \frac{N_A}{A} \sum_i \sigma_i \quad (14)$$

where σ_i is the atomic cross section for the process i , A is the atomic weight and N_A is the Avogadro number. The mass attenuation coefficient, according to Eq. (14) given per g/cm^2 , depends strongly on the photon energy.

2.4.1 Photoelectric effect

Atomic electrons absorb the energy of a photon completely. This effect is not possible for free electrons due to momentum conservation. The absorption of a photon by an atomic electron requires a third collision partner, which in this case is the atomic nucleus. The cross section for absorption of a photon of energy E_γ in the K shell is extremely large ($\approx 80\%$ of the total cross section), because of the proximity of the third collision partner, the atomic nucleus, which absorbs the recoil momentum. The total photoelectric cross section in the non-relativistic range away from the absorption edges is given in the non-relativistic Born approximation by [12]

$$\sigma_{photo}^K = \left(\frac{32}{\epsilon^7} \right)^{1/2} \alpha^4 \cdot Z^5 \cdot \sigma_{Th}^e \left[\text{cm}^2/\text{atom} \right] \quad (15)$$

where, $\epsilon = E_\gamma/m_e c^2$ is the reduced photon energy and

$$\sigma_{Th}^e = \frac{8}{3} \pi r_e^2 = 6.65 \cdot 10^{-25} \text{ cm}^2 \quad (16)$$

is the Thomson cross section for elastic scattering of photons on electrons.

For higher energies ($\epsilon \gg 1$) the energy dependence of the cross section for the photoelectric effect is much less pronounced,

$$\sigma_{photo}^K = 4 \pi r_e^2 \alpha^4 \cdot Z^5 \cdot \frac{1}{\epsilon} \quad (17)$$

In Eqs. (15) and (17) the Z dependence of the cross section is approximated by Z^5 . This indicates that the photon does not interact with an isolated atomic electron. Z -dependent corrections, however, cause σ_{photo} to be a more complicated function of Z . In the energy range between $0.1 \text{ MeV} \leq E_\gamma \leq 5 \text{ MeV}$ the exponent of Z varies

between 4 and 5. As a consequence of the photoelectric effect in an inner shell (e.g., of the K shell) secondary effects may occur, as the free place, e.g., in the K shell, is filled by an electron from a higher shell, the energy difference between those two shells can be liberated in the form of X rays of characteristic energy.

2.4.1.1 Compton scattering

The Compton effect is the scattering of photons off quasi-free atomic electrons. In the study of this interaction process, the binding energy of the atomic electrons is neglected. The total cross section for Compton scattering per electron is given by [12]

$$\sigma_c^e = 2\pi r_e^2 \left\{ \left(\frac{1+\varepsilon}{\varepsilon} \right) \left[\frac{2(1+\varepsilon)}{1+2\varepsilon} - \frac{1}{\varepsilon} \ln(1+2\varepsilon) \right] + \frac{1}{2\varepsilon} \ln(1+2\varepsilon) - \frac{1+3\varepsilon}{(1+2\varepsilon)^2} \right\} [cm^2/electron], \quad \varepsilon = \frac{E_\gamma}{m_e c^2} \quad (18)$$

For Compton scattering off atoms the cross section is increased by the factor Z , because there are exactly Z electrons as possible scattering centers in an atom; consequently $\sigma_c^{atomic} = Z \cdot \sigma_c^e$.

In Compton-scattering process only a fraction of the photon energy is transferred to the electron. Therefore, one defines an energy scattering cross section

$$\sigma_{cs} = \frac{E'_\gamma}{E_\gamma} \cdot \sigma_c^e \quad (19)$$

where, the energy $E'_\gamma = E_\gamma - E_{kin}$ and the E_{kin} is transferred to the target electron.

The Compton scattering is a special effect for photon interactions, because only part of the photon energy is transferred to the target electron, one has to distinguish between the mass attenuation coefficient and the mass absorption coefficient. The mass attenuation coefficient μ_{cs} is related to the Compton-energy scattering cross section σ_{cs} , as in Eq. (19), according to Eq. (14). Correspondingly, the mass absorption coefficient μ_{ca} is calculated from the energy absorption cross-section σ_{ca} , Eq. (14). For various absorbers the Compton-scattering cross sections, or absorption coefficients, have been multiplied by the atomic number of the absorber, since the Compton scattering cross section, Eq. (18), given by the Klein–Nishina formula is valid per electron, but in this case, the atomic cross sections are required.

2.4.2 Pair production

The production of electron–positron pairs in the Coulomb field of a nucleus is only possible if the photon energy exceeds a certain threshold. This threshold energy is given by the rest masses of two electrons plus the recoil energy, which is transferred to the nucleus. From energy and momentum conservation, this threshold energy can be calculated to be

$$E_\gamma \geq 2m_e c^2 + 2 \frac{m_e^2}{m_{nucleus}} c^2 \quad (20)$$

but usually $m_{nucleus} \gg m_e$ the effective threshold can be approximately

$$E_\gamma \geq 2m_e c^2 \quad (21)$$

The pair-production cross section is given by [22]

$$\sigma_{pair} = 4\alpha r_e^2 \cdot Z^2 \left(\frac{7}{9} \ln 2\varepsilon - \frac{109}{54} \right) [cm^2/atom] \quad (22)$$

For large photon energies, the pair-production cross section approaches an energy-independent value which is given approximately by

$$\sigma_{pair} \approx \frac{7}{9} 4\alpha r_e^2 \cdot Z^2 \ln \frac{183}{Z^{1/3}} \approx \frac{7}{9} \cdot \frac{A}{N_A} \cdot \frac{1}{X_0} \quad (23)$$

2.4.3 Total photon absorption cross section and mass attenuation coefficient

Ranges, in which the individual photon interaction processes dominate, are plotted in **Figure 5** as a function of the photon energy and the atomic number of the absorber [11, 12].

The total mass attenuation coefficient, which is related to the cross sections according to Eq. (14), is shown in **Figures 6–9** for the absorbers water, air, Aluminum and Lead [13, 14].

The μ_{ph} is the absorption coefficient for the photoelectric effect, μ_{cs} the Compton scattering, μ_{ca} the Compton absorption and μ_p the pair production. So μ_a is the total mass absorption coefficient ($\mu_a = \mu_{ph} + \mu_p + \mu_{ca}$).

Further interactions of photons (photonuclear interactions, photon–photon scattering, etc.) are governed by extremely low cross sections.

Therefore, these processes are of little importance for the detection of photons. However, these processes are of large interest in elementary particle physics and particle astrophysics.

2.5 Radiation detection

The detection of ionizing radiation in various energy ranges from keV to MeV is presented. The physical processes of radiation/matter interaction have been introduced in the previous text. All the steps of detection are covered, as well as detectors, instrumentations and measurements methods commonly used in the

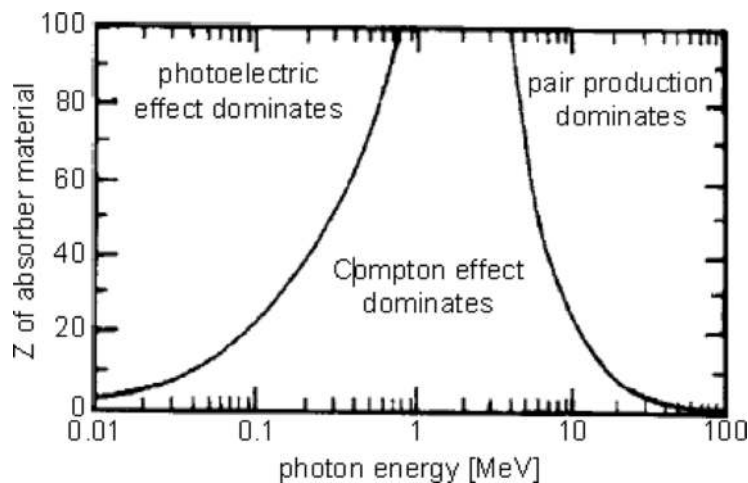


Figure 5. Ranges in which the photoelectric effect, Compton effect and pair production dominate as a function of the photon energy and the target charge number Z [11, 12].

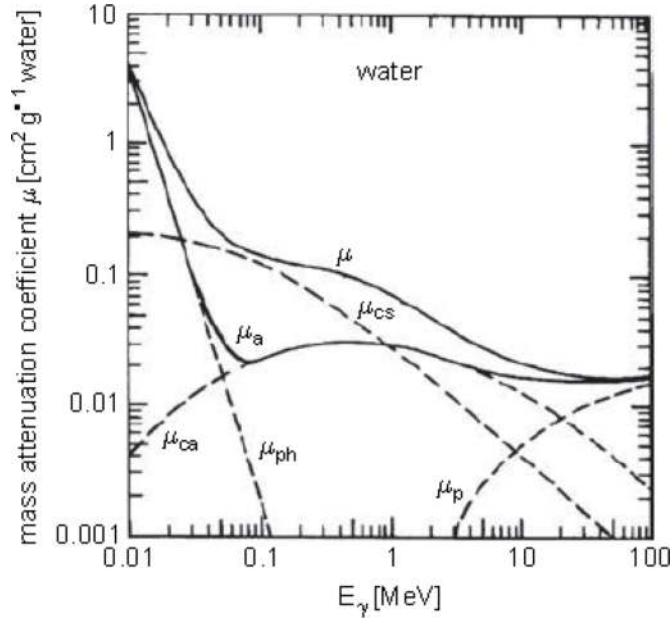


Figure 6.
Energy dependence of the mass attenuation coefficient μ and mass absorption coefficient μ_a for photons in water.

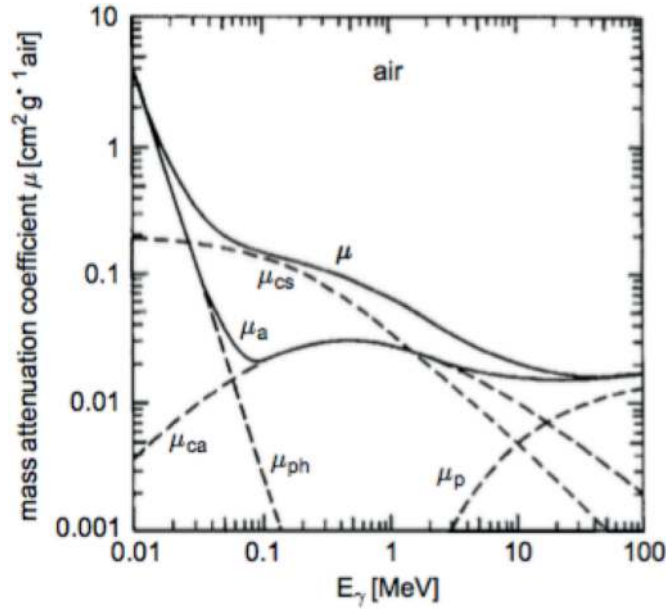


Figure 7.
Energy dependence of the mass attenuation coefficient μ and mass absorption coefficient μ_a for photons in Air.

nuclear field. There are many radiation detectors being developed so far. A selection of the most characteristic detectors will be presented, having played crucial role to the nuclear imaging.

2.5.1 Ionizing chambers

This radiation detector is based on the effects produced by a charged particle passing through a gas. The primary modes of interaction involve ionization and

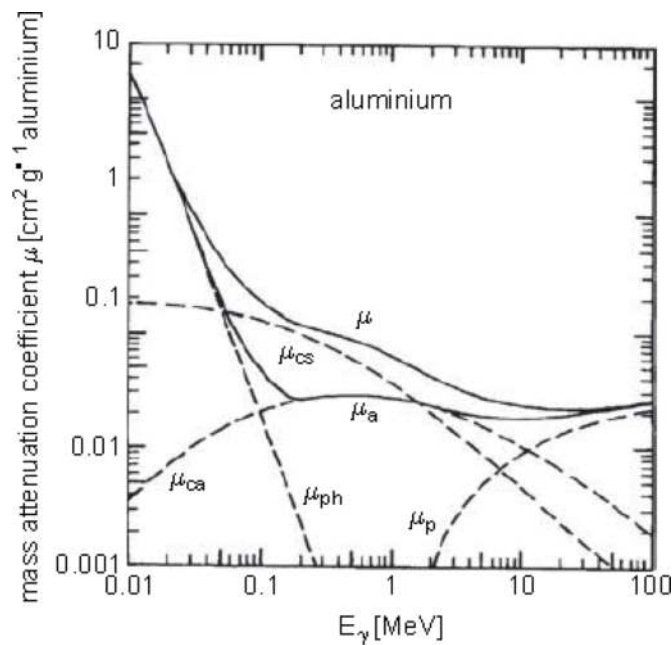


Figure 8.
Energy dependence of the mass attenuation coefficient μ and mass absorption coefficient μ_a for photons in Aluminum.

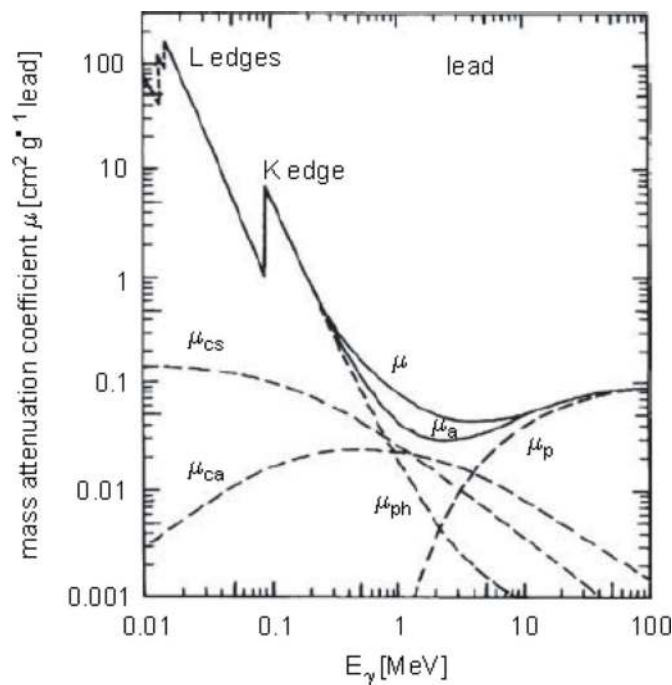


Figure 9.
Energy dependence of the mass attenuation coefficient μ and mass absorption coefficient μ_a for photons in Lead.

excitation of gas molecules along the particle track. An electronic output signal is derived originating from the ion pairs formed within the gas filling the detector. The charged particle transfers an amount of energy equal to the ionization energy of the gas molecule to permit the ionization process to occur. In most gases of interest for radiation detectors, the ionization energy for the least tightly bound electron shells is roughly 10 to 25 eV. The neutral atoms or molecules of the gas are in

constant thermal motion; characterized by a mean free path for typical gases under standard conditions of about 10^6 – 10^8 m. A typical value of the average energy lost by the incident particle per ion pair formed is 25–35 eV/ion pair. Therefore, an incident 1 MeV particle, if it is fully stopped within the gas, will create about 30,000 ion pairs. A point-like collection of free electrons spread around the original point into a Gaussian spatial distribution; where the width increases by the time. An external electric field is applied to the ionization chamber; where ions or electrons created in the gas by the incident particle, electrostatic forces tend to move the charges away from their point of origin. The net motion consists of a superposition of a random thermal velocity together with a net drift velocity in a given direction. The drift velocity for positive ions is in the direction of the conventional electric field, whereas free electrons and negative ions drift in the opposite direction. Finally the total charge collection constitutes an electric current, the called ionization current. The magnitude of the ionization current is too small to be measured usually by a galvanometer. An active amplification of the current is implemented by sensing the voltage drop across a series resistance placed in the measuring circuit. The voltage developed across the resistor (i.e., a value of 10^9 – 10^{12} Ohms) can be amplified used for the measured signal. An alternative approach is to convert the signal from dc to ac at an early stage, which then allows a more stable amplification of the ac signal in subsequent stages. This conversion is accomplished in the dynamic-capacitor or vibrating reed electrometer by collecting the ion current across an RC circuit with long time constant. A charge Q is stored on the capacitance, which is given by $Q = CV$. If a charge ΔQ is created by the radiation, then the total charge stored on the capacitance will be reduced by ΔQ . The voltage will therefore drop from its original value of V_o by an amount ΔV given by.

$$\Delta V = \frac{\Delta Q}{C} \quad (24)$$

A measurement of ΔV provides the total ionization charge or the integrated ionization current over the period of the measurement.

2.5.2 Scintillator detectors

Scintillation detectors offer one possibility of providing a solid detection medium, and their application to the detection and measurement of various radiations. The detection of ionizing radiation by the scintillation light produced in certain materials is a very well established technique and remains one of the most useful methods available for the detection and spectroscopy of a wide variety of radiations. The kinetic energy of charged particles is converted into detectable light, by subsequent photosensitive detector, with high scintillation process efficiency. The conversion is taken care to be linear and the light yield to be proportional to the deposited energy over the most possible wide range. The scintillating material should be transparent to the wavelength of its own emission for total light collection. The decay time of the induced luminescence is short and then fast signal pulses can be generated. The process of fluorescence is the prompt emission of visible radiation from a substance following its excitation by incident radiation. It is conventional to distinguish several other processes that can also lead to the emission of visible light. The scintillation efficiency of any scintillator is defined as the fraction of all incident particle energy, which is converted into visible light. The rise and fall of the light output can be characterized by the full width at half maximum (FWHM) of the resulting light versus time profile, which can be measured using

very fast timing procedures. It has become common to specify the performance of ultrafast organic scintillators by their FWHM time rather than the decay time alone. It is noted that both rise and decay time are of the order of ns. The alkali halide scintillators as the Sodium Iodide with trace of Thallium NaI(Tl) and the Cesium Iodide with trace of Thallium or Sodium CsI(Tl)/CsI(Na) are so broadly implemented for gamma spectroscopy and medical imaging applications. An alternative scintillation material, Bi₄Ge₃O₁₂ (BGO) is available as crystals of reasonable size. A major advantage is the high density (7.13 g/cm³) and the large atomic number (83) of the Bismuth element. These properties result in the largest probability per unit volume for the photoelectric absorption of gamma rays. Its physical properties make it easy to handle and use. The light yield from BGO is relatively low, being variously reported at 10–20% of that of NaI(Tl).

2.5.3 Si/Ge solid state detectors

The use of a solid detection medium in many radiation detection applications is of great advantage, as for the measurement of high-energy electrons or gamma rays. The detector dimensions can be kept much smaller than the equivalent gas-filled detector because the solid densities are some 1000 times greater than that for a gas. The use of semiconductor materials as radiation detectors can result in a much larger number of carriers for a given incident radiation event than is possible with any other common detector type, described previously. Consequently, the best energy resolution from radiation spectrometers is achieved using semiconductor detectors. The fundamental information carriers are electron-hole pairs created along the path taken by the charged particle of the primary radiation or secondary particle through the detector. The electron-hole pair is somewhat analogous to the ion pair created in gas-filled detectors. Their motion in an applied electric field generates the basic electrical signal from the detector. Under low values of the electric field intensity, the drift velocity v is proportional to the applied field. Then a mobility μ for both electrons and holes can be defined by.

$$v_e = \mu_e E \quad v_h = \mu_h E \quad (25)$$

where, E is the electric field magnitude. We have seen, that the mobility of the free electron in the gas is much larger than of the positive ion, but in semiconductor materials the mobility of the electron and hole are roughly of the same order, saturated by the increased electric field to value of the order of 10^7 cm/s. When a charged particle passes through a semiconductor the overall significant effect is the production of many equal numbers electron-hole pairs along the track of the particle. The process produces high-energy electrons or delta rays that subsequently lose their energy in producing more electron-hole pairs. This quantity, is called the ionization energy, is experimentally observed to be largely independent of both the energy and type of the incident radiation, provided the charge particle is fully stopped within the active volume of the detector.

The Si surface barrier detectors have widespread application for the detection of alpha particles and other short-range radiations but are not easily adaptable for applications that involve more penetrating radiations. Their major limitation is the maximum depletion depth or active volume that can be created. Using Silicon or Germanium of normal semiconductor purity, depletion depths beyond 2 or 3 mm are difficult to achieve despite applying bias voltages that are near the breakdown level. A low impurity concentration corresponds to levels that are less than 1 part in 10¹², a virtually unprecedented degree of material purity. Techniques have been

developed to achieve this goal in Germanium, but not in Silicon. The process of Lithium ion drifting has been applied in both Silicon, Si(Li), and Germanium, Ge(Li), crystals to compensate the material after the crystal has been grown. Detectors that are manufactured from this ultrapure Germanium are usually called high purity Germanium (HPGe) detectors, and they have become available with depletion depths of several centimeters. The room-temperature operation of Germanium detectors is impossible because of the large thermally induced leakage current, due to the small band gap (~ 1 eV). So, the Germanium detectors must be cooled to reduce the leakage current to the point that the associated noise does not spoil their excellent energy resolution. Normally, the operation temperature is at 77 K through the use of an insulated Dewar vessel, which a reservoir of liquid Nitrogen is kept in thermal contact with the detector. For Ge(Li) detectors, the low temperature must be maintained continuously to prevent a catastrophic redistribution of the drifted lithium that will rapidly take place at room temperature.

2.5.4 Pixel detectors

The approach to obtain two-dimensional position information from a single sided silicon detector is to fabricate the top electrode as a checkerboard pattern of individual small elements that are electrically isolated from each other. If the electrode dimensions are smaller than 1 mm, the common terminology is pixel detector. Electrical connection must be made to each individual electrode and separate electronic readout channels provided for each. This approach has the advantage that the small size of each individual electrode results in a relatively small capacitance and leakage current, and thus the electronic noise is reduced considerably from that observed from microstrip detectors of equivalent dimensions. In the usual approach, a pixel detector chip is connected to a separate readout chip using flip chip solder bonding or Indium bump bonds. The readout chip is fabricated with exactly the same pitch as the detector pixels, so each bump provides an electrical connection between a single pixel and its corresponding readout electronics. Pixel detectors typically have active areas that are limited to the order of square centimeters. Larger detector areas can be achieved by assembling individual modules into arrays, although at the expense of increasing complexity in what is already a complex device.

2.6 Electronics and DAQ

Complicated electronic systems are adapted to get the information of the signal extraction by the radiation detectors. After an analog and digital treatment of the detector plus electronics waveform; a data acquisition system (DAQ) is accumulating the data for further analysis and study.

2.6.1 Signal processing and analysis: types of electronics, signal collection and amplification, particle discrimination, spatial and time resolution

It is often desirable to change the shape of the pulse signal from radiation detectors, in some predetermined fashion. It is the most common application in processing a train of pulses produced by a preamplifier. In order to ensure that complete charge collection occurs, preamplifiers are normally adjusted to provide a decay time for the pulse, which is quite long, typically 50 μ s. Depending of the rate of interaction in the detector these pulses will tend to overlap one another and give rise to a pulse train. The ideal shape is to eliminate the long tails of the pulses, but

the information carried by the maximum amplitude of the pulse has been preserved. The pulses have been shaped in the sense that their total length has been reduced drastically but not affecting the maximum amplitude. The nuclear pulse shaping, it is conventional to make an important distinction between differentiator or CR networks and integrator or RC. Both operations can also be thought of as filtering in the frequency domain, for pulse shaping to improve signal-to-noise ratio by limiting the response of the instrumentation to those frequency ranges in which the signal has useful components. This type of pulse shaping is conventionally carried out in the linear amplifier element of a nuclear pulse signal chain and then to the digital pulse processing, for getting a digitized version of the input waveform for further analysis. A linear pulse is defined as a signal pulse that carries information through its amplitude, and sometimes by its shape as well. A sequence of linear pulses may therefore differ widely in size and shape characteristics. In addition, a logic pulse is a signal pulse of standard size and shape that carries information only by its presence or absence, or by the precise time of its appearance. Usually, all radiation detector signal chains start out with linear pulses, which after passing fixed amplitude discrimination, a digital conversion provides the logic pulses by the ADC (Analog to Digital Converter) elements. The information on the precise arrival time of a quantum of radiation in the detector is of particular interest. The accuracy of the timing information to be performed depends both on the properties of the specific detector, where the signal charge is collected rapidly and the type of electronics used to process the signal. The timing characteristics of a certain system depend greatly on the dynamic range, ratio of maximum to minimum pulse height, of the signal pulses. The time resolution is defined by the time measurement accuracy of the system. Similar spatial resolution of a nuclear chain is defined for acquiring the discrimination of two same radiation quanta passing in nearby places of a detector.

2.6.2 Multi-channel analysis and measurements: principle of measurements, spectrometry, common detection instrumentations, applications in nuclear engineering and R&D

A measurement of the differential pulse height spectrum from a radiation detector can yield important information on the nature of the incident radiation or the properties of the detector itself and is therefore one of the most important functions to be performed in nuclear measurements. By definition, the differential pulse height spectrum is a continuous curve that plots the value of dN/dH , the differential number of pulses observed within a differential increment of pulse height H , versus the value of the pulse height H .

The multichannel analyzer (MCA) is comprised of basic electronics components chain setup. The major task of its operation is based on the principle of converting an analog signal (the pulse amplitude) to an equivalent digital number. Then, an extensive technology available for the storage and display of the digital information provides the recording pulse height spectra. As a result, the analog to-digital converter (ADC) is a key element in determining the performance characteristics of the analyzer.

The nuclear instrumentation, mainly, based by the detector, the electronic system, the MCA and the data storage-analysis medium, can be properly adapted for several applications. Those applications are starting from the nuclear engineering instrumentation for nuclear reactors monitoring and safety, to various research instrumentations for accelerators or detector systems and so on. All these

experience of the nuclear instrumentation, accumulated the last decades, is implemented to the medical applications and indeed to the nuclear medical imaging techniques.

3. The X-ray computed tomography imaging

The X-rays are high-energy photons produced via special vacuum tubes. The X-rays are proportionally attenuated when passing through various media; being the major advantage for the X-ray imaging. The updated medical diagnosis result of this technology is the three-dimensional (3D) X-ray computed tomography (CT), used in medical diagnosis.

3.1 X-ray generation and interaction with matter

A typical X-ray tube consists of a cathode providing, by thermal emission, beam of electrons accelerated due to the anode voltage. Kinetic energy loss of the electrons at an anode is converted to X-rays. The relative position of the excited electron in the anode determines the frequency and energy of the emitted X-ray. The X-rays interact with matter in several ways, as the photon interaction mechanisms, reported in paragraph 1.4; meaning the Photoelectric effect, Compton scattering and Pair production. The major effect in diagnostic imaging is the photoelectric effect; where an orbital electron, mainly for elements of large atomic number, absorbs the energy of an X-ray photon.

3.2 CT imaging

The established X-ray imaging technique is useful for clinical diagnosis in cases of a view of the bone system. The technique offers only low soft-tissue contrast and is not very quantitative. The X-ray CT tomography relies on taking a large number of X-rays at multiple angles, getting many measurements of the incident X-ray attenuation through the plane of the human body. The attenuation measurements provide the fraction of X-ray removed in passing through a given amount of a specific material of thickness. The data obtained provide the X-ray tomography information and reconstruct a 3D image after a heavy and well elaborated data processing. The computed tomography (CT) is the method for reconstructing and providing the image of a thin cross section on the basis of measurements of X-ray attenuation. Instead, the plain film X-ray image, CT images are free of superimposing tissues and are capable of much higher contrast due to elimination of scatter. Major upgrading improvements have led to higher-resolution images, which the diagnosis process. The small size nodules or tumors can be visualized, by the CT scan, which they could not be seen with a plain X-ray film. To help soft tissues providing clear image, a special contrast material is needed to block the X-rays, in a CT scan, so highlighting blood vessels, organs, or other structures.

4. The nuclear medicine SPECT, PET and PET-CT tomography imaging

Nuclear medicine is a branch of medical imaging applying non-invasive, diagnostic imaging techniques for visualization of internal organs, tissue, etc. and monitoring the functioning of them. Major modalities of imaging are the X-ray Radiography (projection), the X-ray Computed Tomography (CT) and the Nuclear Medicine (SPECT, PET and PET-CT) [15, 16]. The injected radioactive tracers

(radiopharmaceuticals) to human body assess tissue functions and to diagnose and treat properly various diseases but mainly malignant tissues. Specially designed cameras track the path of these radioactive tracers. Single Photon Emission Computed Tomography or SPECT and Positron Emission Tomography or PET scans are the two most common imaging modalities in nuclear medicine. The PET-CT scan is a combination of the PET and the CT-computed tomography, described above, which give excellent results of the cancer spots inside the body not viewed via PET or CT separately. Approved tracers are called radiopharmaceuticals since they must meet FDA's² or EMA's³ exacting standards for safety and appropriate performance for the approved clinical use. The proper tracer is selected to provide the most specific and reliable information for a patient's particular problem. The used tracer is determined by the SPECT or PET scan to be applied to the patient [17].

4.1 SPECT imaging

The SPECT imaging scanner provides three-dimensional tomographic images of the distribution of radioactive tracer molecules that have been introduced into the patient's body. The 3D images are computer generated from a large number of projection images of the body recorded at different angles. The SPECT imagers have gamma camera detectors that can detect the gamma ray emissions from the tracers that have been injected into the patient [18]. The camera sensor detectors are mounted on a rotating gantry that allows them to be moved in a tight circle around a patient who is lying motionless on a moving bed [19]. The SPECT scans are primarily used to diagnose and track the progression of heart disease, such as blocked coronary arteries. There are also radiotracers to detect disorders in bone, gall bladder disease and intestinal tuberculosis or bleeding. The SPECT agents have recently become available for aiding in the diagnosis of Parkinson's disease in the brain, and distinguishing this disease from other anatomically related movement disorders and dementias [20]. The gamma camera has usually a set of photomultipliers on a scintillating crystal in front of which the collimator defines the image quality to be obtained, **Figure 10**. The collimator localizing the origin of the gamma ray forms a projection image by allowing only those gamma rays traveling in certain directions to reach the scintillating crystal.

4.2 PET imaging

The PET scan also uses special radiopharmaceuticals to create three-dimensional images. These radiopharmaceuticals are labeled with radioisotopes (^{11}C , ^{18}F , ^{15}O or ^{13}N) of very short life-time (~minutes to few hours) and they emit positrons by their decay. The positrons are anti-particles of the electrons having positive charge. The positrons with electrons annihilate each other, in the human tissue where have been injected, emitting two gamma rays of equal energy 512 keV each in opposite directions due to the conservation of energy and momentum [20, 21]. The detectors in the PET scanner facility measure these photons emitted in time coincidence and in 180° angle. The PET camera also allows determining where they two photons are coming from, the position of the nucleus when it decayed, and also knowing where the nucleus moves inside the body. The data of the detectors obtained are processed for providing the information to create images of internal organs or tissues.

² FDA: U.S. FOOD & DRUG ADMINISTRATION, <https://www.fda.gov/MedicalDevices/NewsEvents/WorkshopsConferences/ucm429282.htm>

³ EMA: EUROPEAN MEDICINES AGENCY, <https://www.ema.europa.eu/>

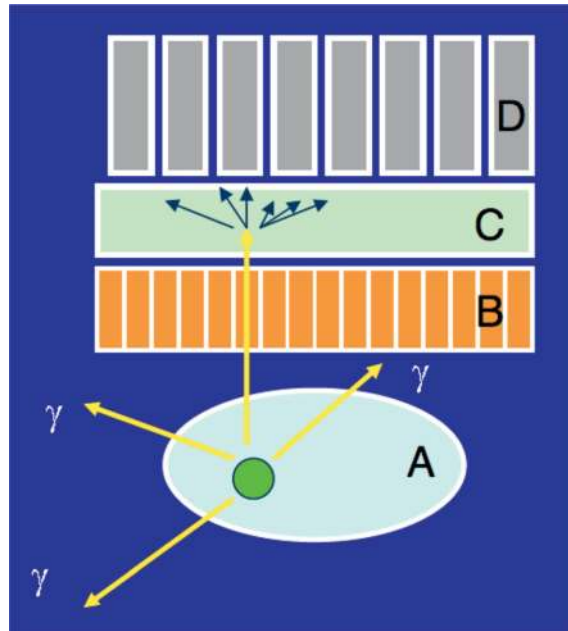


Figure 10.

The gamma camera setup (principle), A is the organ, and under examination, with the radiopharmaceutical compound emitting gamma rays, B is the collimator, C is the scintillating crystal and D is the array of the photomultipliers.

The PET scan is mainly used for the patients with conditions affecting the brain, heart, certain types of cancer, Alzheimer's disease and some neurological disorders. The major purpose of PET scans is to detect cancer and monitor its progression, response to treatment, and to detect metastases. Glucose utilization depends on the intensity of cellular and tissue activity so it is greatly increased in rapidly dividing cancer cells. In the last years, slightly modified radiolabeled glucose molecules (F-18 labeled deoxyglucose or FDG) have been shown to be the best available tracer for detecting cancer and its metastatic spread in the body. Different colors or degrees of brightness on a PET image represent different levels of tissue or organ function. The healthy tissues use glucose for energy, accumulating some of the tagged glucose, which will show up on the PET images. However, the tumors use more glucose than normal tissue, accumulate more of the substance and appear brighter than normal tissue on the PET images.

4.3 PET-CT imaging

A combination instrument that produces both PET and CT scans of the same body regions in one examination (PET/CT scanner) has become the primary imaging tool for the staging of most cancers worldwide. The images of the PET and the PET-CT combined are shown in **Figure 11** [22]; where the results of the PET-CT image are extremely interesting. The incremental diagnostic value of integrated positron emission tomography-computed tomography (PET/CT) compared with PET tomography are summarized: (i) imaging quality improvement in tumors detection on both CT and PET, (ii) imaging quality improvement to the loci up taking tracer in better ratio between physiological from pathologic tissue, (iii) precise localization of the malignant foci, in various body places, i.e., bones, soft tissues, etc. (iv) improvement of spatial resolution for defining small size or unusual tumors. The use of PET/CT technique can occur at the time of initial diagnosis, in assessing the early response of disease to treatment, at the conclusion of treatment, and in continuing follow-up of patients. The PET/CT fused images

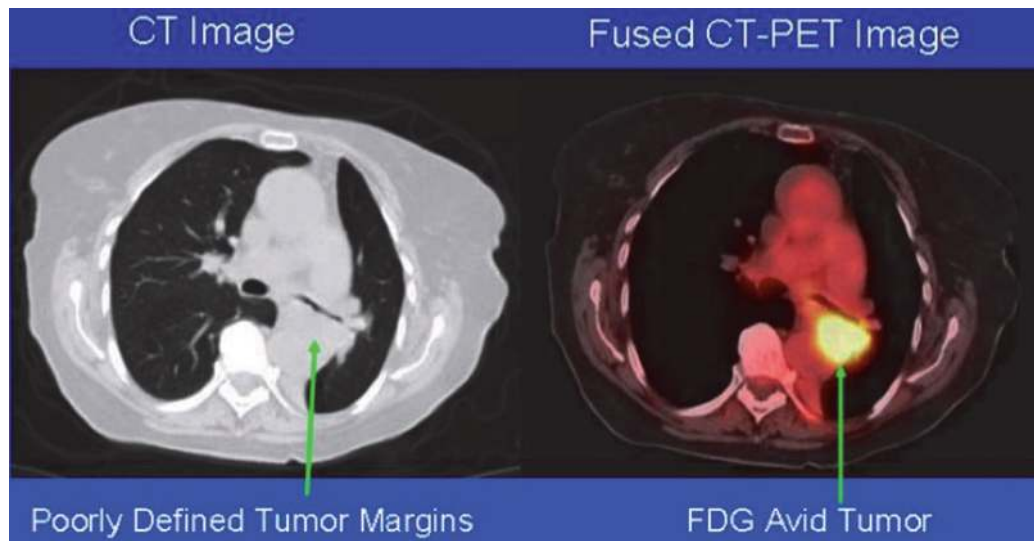


Figure 11.
The comparison between the CT image and the combined PET-CT image; where the avid tumor is well and clearly viewed on the right image (<https://www.nibib.nih.gov/>) [22].

have the potential to provide important information to guide the biopsy of a mass to active regions of the tumor and to provide better tissue mapping [22]. The wide array of clinical applications of ionizing radiation is grouped into diagnostic and therapeutic use [23].


The radiation dose and the diagnostic radiology procedures are of concern to the health care professions, the public, and regulators. The radiation dose depends on various factors, including the weight of the patient, the radiation sensitivity of the image tissue receptor, the energy of the radiation, the exposure rate, and the total time of radiation. Measurements of equivalent collective dose are taken for the individual patients and populations. The radiation dose from nuclear medicine procedures depends on the radiopharmaceutical, the administered activity, and individual patient metabolism. For clinical applications, dosimetry estimates of radiopharmaceuticals are provided based on standardized adult and child metabolic and anatomic models. Recently, the use of electron accelerators as radiation source equipped with an X-ray converter is increasing. However, gamma sources are difficult to replace, especially for use with non-uniform, high-density products [24]. Fourth generation of light sources are the X-ray free electron lasers (XFELs) [25]. They provide bright bursts of X-rays, where these pulses are both spatially coherent and ultra short in duration. New techniques have been developed, including diffract-before-destruction methods; where the short X-ray pulse scatters from the sample, providing the radiation-damage-free structures measurement. They have been applied to develop a technique called serial femtosecond crystallography (SFX), where a stream of tiny protein crystals is delivered into the focus of the XFEL [26]. The Crystal Clear is an international collaboration at CERN, active on research and development on inorganic scintillation materials for novel ionizing radiation detectors, for high-energy physics, better quality medical imaging (PET-SPECT) and industrial applications [27].

Author details

Evangelos Gazis
National Technical University of Athens, Athens, Greece

*Address all correspondence to: evangelos.gazis@cern.ch

IntechOpen

© 2019 The Author(s). Licensee IntechOpen. This chapter is distributed under the terms of the Creative Commons Attribution License (<http://creativecommons.org/licenses/by/3.0>), which permits unrestricted use, distribution, and reproduction in any medium, provided the original work is properly cited. 

References

- [1] Enge H. Introduction to Nuclear Physics. Boston: Addison-Wesley; 1972
- [2] Kleinknecht K. Detectors for Particle Radiation. Cambridge UK: Cambridge University Press; 1986
- [3] William R. Leo, Techniques for Nuclear and Particle Physics Experiments. 2nd ed. Berlin, Heidelberg, New York: Springer Verlag; 1994
- [4] Knoll GF. Radiation Detection and Measurement. 3rd ed. New York: John Wiley & Sons; 1999
- [5] Sitar B, Merson GI, Chechin VA, Budagov YA. Ionization Measurements in High Energy Physics. Springer Tracts in Modern Physics. Vol. 124. Berlin/Heidelberg: Springer; 1993
- [6] Bethe HA. Theorie des Durchgangs schneller Korpuskularstrahlen durch Materie. Annalen der Physik. 1930;5: 325-400
- [7] Bloch F. Bremsvermögen von Atomen mit mehreren Elektronen. Zeitschrift für Physik. 1933;81:363-376
- [8] Uehling EA. Penetration of heavy charged particles in matter. Annual Review of Nuclear and Particle Science. 1954;4:315-350
- [9] Particle Data Group. Review of particle properties. Physical Review D. 2018;98:030001
- [10] Marshall JS, Ward AG. Absorption curves and ranges for homogeneous β -rays. Canadian Journal of Research. 1937;A15:39-41
- [11] Sauter E. Grundlagen des Strahlenschutzes. Berlin/München: Siemens AG; 1971. Grundlagen des Strahlenschutzes. Thieme/München; 1982
- [12] Marmier P, Sheldon E. Physics of Nuclei and Particles. Vol. 1. New York: Academic Press; 1969
- [13] Evans RD. The Atomic Nucleus. New York: McGraw-Hill; 1955
- [14] Grodstein GW. X-Ray attenuation coefficients from 10 keV to 100 MeV. National Bureau of Standards Supplement to Circular. 1957;583:1
- [15] Hine GJ. Instrumentation in Nuclear Medicine. 1st ed. Cambridge MA: Academic Press; 1967
- [16] Alazraki NP, Mishkin FS. Fundamentals of Nuclear Medicine. 2nd ed. New York: The Society of Nuclear Medicine; 1988
- [17] Edward L. Alpen, Radiation Biophysics. 2nd Edition. San Diego CA: Academic Press; 1998
- [18] Khoshakhlagh M et al. Development of scintillators in nuclear medicine. World Journal of Nuclear Medicine. 2015;14(3):156-159
- [19] Fockler A, Voslar A, Guibault J. Spatial resolution of gamma cameras for whole body bone imaging. Journal of Nuclear Medicine. 2016;57 (Supplement 2):2828
- [20] Webb A. Introduction to Biomedical Imaging. Hoboken NJ: John Wiley & Sons; 2003
- [21] Hendee WR, Ritenour ER. Medical Imaging Physics. 4th Edition. New York: Wiley; 2002
- [22] NIBIB-National Institute of Biomedical Imaging and Bioengineering Health & Human Services. Available from: <https://www.nibib.nih.gov/science-education/science-topics/nuclear-medicine>

[23] Gottfried K-LD, Penn G, editors. Radiation in Medicine, A Need For Regulatory Reform, Institute of Medicine (US) Committee for Review and Evaluation of the Medical Use Program of the Nuclear Regulatory Commission. Washington DC: National Academic Press; 1996

[24] Sun Y, Chmielewski AG. Chapter: Future developments in radiation processing. In: Applications of Ionizing Radiation in Materials Processing. 1st ed. Warszawa: Institute of Nuclear Chemistry and Technology; 2017

[25] Pellegrini C, Marinelli A, Reiche S. The physics of X-ray free-electron lasers. Reviews of Modern Physics. 2016;**88**:015006

[26] Martin-Garcia JM et al. Serial femtosecond crystallography: A revolution in structural biology. Archives of Biochemistry and Biophysics. 2016;**602**:32-47

[27] Medjoubi K et al. Performances and Applications of the CdTe- and Si-XPAD3 photon counting 2D detector. Journal of Instrumentation. 2011;**6**:C01080